Am J Physiol Gastrointest Liver Physiol 319: G733–G747, 2020.
First published October 14, 2020; doi:10.1152/ajpgi.00094.2020.

RESEARCH ARTICLE | *Nutrient Sensing, Nutrition, and Metabolism*

Differential expression of full-length and NH_2 terminally truncated FAM134B isoforms in normal physiology and cancer

Umur Keles,[1,2] Evin Iscan,[1,2] Huriye Erbak Yilmaz,[2] Gökhan Karakülah,[1,2] Aslı Suner,[3] Erhan Bal,[1] Nilgun Tasdemir,[4] Ayse Derya Cavga,[4] Umut Ekin,[1,2] Zeynep Mutlu,[1] Sila Kahyaoglu,[1] Muhittin A. Serdar,[5] Nese Atabey,[1] and Mehmet Ozturk[1]

[1]*Izmir Biomedicine and Genome Center, Izmir, Turkey;* [2]*Izmir International Biomedicine and Genome Institute, Dokuz Eylul University, Izmir, Turkey;* [3]*Department of Biostatistics and Medical Informatics, Ege University, Izmir, Turkey;* [4]*Department of Molecular Biology and Genetics, Bilkent University, Ankara, Turkey; and* [5]*Department of Biochemistry, Acıbadem University, İstanbul, Turkey*

Submitted 30 March 2020; accepted in final form 4 October 2020

Keles U, Iscan E, Yilmaz HE, Karakulah G, Suner A, Bal E, Tasdemir N, Cavga AD, Ekin U, Mutlu Z, Kahyaoglu S, Serdar MA, Atabey N, Ozturk M. Differential expression of full-length and NH_2 terminally truncated FAM134B isoforms in normal physiology and cancer. *Am J Physiol Gastrointest Liver Physiol* 319: G733–G747, 2020. First published October 14, 2020; doi:10.1152/ajpgi.00094.2020.—Selective autophagy of the endoplasmic reticulum (ER), namely ER-phagy, is mediated by ER-localized receptors, which are recognized and sequestered by GABARAP/LC3B-decorated phagophores and transferred to lysosomes for degradation. Being one such receptor, *FAM134B* plays critical roles in cellular processes such as protein quality control and neuronal survival. *FAM134B* has also been associated with different cancers, although its exact role remains elusive. We report here that the *FAM134B* gene encodes not one but at least two different protein isoforms: the full-length and the NH_2 terminally truncated forms. Their relative expression shows extreme variation, both within normal tissues and among cancer types. Expression of full-length FAM134B is restricted to the brain, testis, spleen, and prostate. In contrast, NH_2 terminally truncated FAM134B is dominant in the heart, skeletal muscle, kidney, pancreas, and liver. We compared wild-type and knockout mice to study the role of the *Fam134b* gene in starvation. NH_2 terminally truncated FAM134B-2 was induced in the liver, skeletal muscle, and heart but not in the pancreas and stomach following starvation. Upon starvation, *Fam134b*$^{-/-}$ mice differed from wild-type mice by less weight loss and less hyperaminoacidemic and hypocalcemic response but increased levels of serum albumin, total serum proteins, and α-amylase. Interestingly, either NH_2 terminally truncated *FAM134B* or both isoforms were downregulated in liver, lung, and colon cancers. In contrast, upregulation was observed in stomach and chromophobe kidney cancers.

NEW & NOTEWORTHY We reported tissues expressing FAM134B-2 such as the kidney, muscle, heart, and pancreas, some of which exhibit stimulated expression upon nutrient starvation. We also demonstrated the effect of *Fam134b* deletion during ad libitum and starvation conditions. Resistance to weight loss and hypocalcemia, accompanied by an increase in serum albumin and α-amylase levels, indicate critical roles of *Fam134b* in physiology. Furthermore, the differential expression of FAM134B isoforms was shown to be significantly dysregulated in human cancers.

autophagy; endoplasmic reticulum; ER-phagy; gene expression; gene knockout; hepatocellular carcinoma; reticulophagy

INTRODUCTION

FAM134B (also called RETREG1) is a critical gene for neuronal survival. *FAM134B* loss-of-function mutations cause hereditary sensory and autonomic neuropathy type II, and its knockdown results in structural alterations of the *cis*-Golgi compartment, inducing apoptosis in some primary dorsal root ganglion neurons (25). This pathology is associated with a major role of FAM134B in selective endoplasmic reticulum (ER) degradation by autophagy, or ER-phagy. Mutant FAM134B proteins that cause sensory neuropathy in humans (25) are also unable to act as ER-phagy receptors (22). The autophagy receptor FAM134B is tethered to the ER membrane by its reticulon-homology domain (RHD), which is composed of two large transmembrane domains (TM12 and TM34), and binds to phagophore-associated LC3/GABARAB proteins via its COOH terminally located LC3-interacting region (LIR) motif (6, 22).

FAM134B was shown to mediate lysosomal degradation of bulk ER fragments during starvation (22) or during ER stress response caused by misfolded luminal proteins (13, 14). On the other hand, FAM134B overexpression was found to induce ER stress, followed by cell death in HeLa cells (27). Early studies also reported that *FAM134B* expression is enhanced in fatty pig adipocytes and that its experimental overexpression induced lipid deposition (43). Recently, the overexpression of *FAM134B* in mouse white adipose tissue was reported to increase obesity by promoting adipogenesis via enhanced mitophagy (8).

There are also several reports linking *FAM134B* to different cancer types as both a tumor suppressor and promoter. Initially, *FAM134B* was described as an oncogene that is able to transform the mouse NIH 3T3 cell line and found to be overexpressed in human esophageal cancer (38). Additional studies showed that its experimental downregulation induces significant reductions in cell proliferation, colony formation, wound healing, migration, and invasion capacities of esophageal cancer cells (19). On the other hand, *FAM134B* displayed features of a tumor suppressor in colon cancer, since lower levels of the *FAM134B* protein expression are associated with larger tumor size, advanced cancer stages, and higher recurrence rates (21). In breast cancer, the *FAM134B* expression is relatively higher in estrogen receptor-positive or nontriple negative subtypes and positively correlated with patient relapse-free survival, which is suggestive of a tumor suppressor role (11). In further support of

Correspondence: M. Ozturk (mehmet.ozturk@ibg.edu.tr).

a tumor-suppressive role, we also identified *FAM134B* as a hepatocellular senescence-associated gene, serving as a robust biomarker for the differentiation of hepatocellular carcinoma (HCC) from cirrhosis (42). In contrast, Zhang et al. (45) recently reported a highly elevated expression of *FAM134B* in HCC compared with normal liver tissues. In addition, HCC patients with a higher expression of *FAM134B* have shorter overall survival and disease-free survival. Experimentally, the knockdown of *FAM134B* with shRNA inhibits cell growth and motility, as well as tumor formation and metastasis in nude mice, and its overexpression leads to increased cell proliferation and motility, as well as increased tumor formation and metastasis (45).

Given the discordant and controversial reports on the biological roles of FAM134B in literature, herein we performed a detailed exploration of this interesting gene by in silico, in vitro, and in vivo approaches in terms of its structure, expression, and implications in both normal physiology and cancer.

METHODS

Genome and transcriptome data. The illustration of human and mouse FAM134B transcript variants was recreated using the National Center for Biotechnology Information reference sequence (RefSeq) database with the following accession codes: human FAM134B-1, NM_001034850.2; human FAM134B-2, NM_019000.4; mouse isoform-1, NM_001034851.2; mouse isoform-2, NM_025459.3; mouse isoform-3, NM_001277315.1; mouse isoform-4, NM_001277316.1; mouse isoform-5, NM_001277317.1; and mouse isoform-6, NM_001277318.1. The exon annotation was based on the University of California Santa Cruz (UCSC) genome browser.

The expression data of FAM134B variants in human healthy tissues were retrieved from the Genotype Tissue Expression (GTEx) database, version 3 as reads per kilobase million (RPKM) values (3). Bar graphs were generated using Log2 (RPKM + 1) excluding the standard deviation.

Cancer and normal tissue expression data of human FAM134B isoforms were downloaded directly from The Cancer Genome Atlas Splicing Variant Database (TSVdb) as RNA-Seq by Expectation Maximization (RSEM) values (36). This database provides isoform level expression value of any human gene across 33 tumor types, and researchers can retrieve and interpret the isoform expression variations between or across clinical subgroups. Statistical analyses of tumor and nontumor groups were performed using the nonparametric Mann-Whitney *U* test, and $P < 0.01$ was accepted as significant.

Protein alignment and modeling. Human, mouse, and bovine amino acid sequences of FAM134B isoforms were obtained from the UCSC Genome Browser. The sequences were aligned utilizing the alignment function of UniProt (5), and the reticulon domains of FAM134B were predicted through the PSIPRED workbench (7), using MEMSAT transmembrane topology prediction method (32). The LC3B binding LIR motif had previously been identified, and the homolog LIR amino acid sequence was used for illustration.

Reverse transcriptase-polymerase chain reaction. Total RNA from tissues were extracted using the NucleoSpin RNA isolation kit (Macherey-Nagel) and converted to cDNA using the RevertAid First Strand cDNA Synthesis Kit (ThermoFisher) as per manufacturer's instructions. The PCR was set up in a 20-μl reaction mixture with total 20 ng of cDNA per reaction by using the MyTaq DNA polymerase kit (Bioline). The oligonucleotide sequences for human FAM134B isoforms were as follows: hFAM134B-1-F, 5′-GAGAAGCCTCAGTGAAAGCTG-3′; hFAM134B-2-F, 5′-TTTGGACCAGGCAAAAGCTGG-3′; and hFAM134B-Common-R, 5′-GCAACCGTGAGGCTAATCTTAGGA-3′. The oligonucleotides used for mouse *Fam134b* mRNA isoforms were as follows: isoform1-F, 5′-TTCTGGTTCCTTGCCTTGAC-3′; isoform2-F, 5′-TGCTGGAGTGAGAGAGCCTGT-3′; isoform3-F, 5′-CATAATAGTCCACTCCTCGGC-3′; isoform4-F, 5′-TCACGGTGCTGGAGTGAGAGC-3′; isoform5-F, 5′-CTCTGAGGTAATAGGCTCCTG-3′; isoform6-F, 5′-AGTGTTATGAAATGGGTCACAG-3′; common reverse, 5′-CAGAAGGTAGCTGAGTATGAC-3′; isoformX common-F, 5′-TCCTGTGCGTGCTTCTTGTGAG-3′; isoformX1-R, 5′-AAGCGCTCCTCCTCTCTC-3′; isoformX2-R, 5′-AAAGCGCTCCTCCTCTAC-3′; HPRT-F, 5′-CACAGGACTAGAACACCTGC-3′; and HPRT-R, 5′-GCTGGTGAAAAGGACCTCT-3′.

The RT-PCR was performed under the following conditions: 3 min at 94°C (initial denaturation), 1 cycle; 30 s at 94°C (denaturation), 30 s at 58°C (annealing), 30 s at 72°C (extension), 35 cycles; 3 min at 72°C (final extension), 1 cycle. Samples were run at 1.5% agarose gel for 45 min at 90 V using Tris acetic acid EDTA in both agarose gel and running buffer. The DNA was stained with SafeView (ABM, Inc.) by adding into both the agarose gel and the running buffer.

Ethical statement. All animal experiments were approved by the Izmir Biomedicine and Genome Center Animal Experiments Local Ethics Committee (IBG-AELEC). Human samples used in the RT-PCR were approved by the Ethics Committee of Dokuz Eylul University. Written consent was obtained from all patients before liver transplantation.

Animal studies. The *Fam134b*$^{+/-}$ mice (22) were a kind gift from Christian Hübner. Male and female mutant mice, along with their wild-type counterparts, were housed and bred in individually ventilated cages (IVC) under a 12-h light-dark cycle at 22 ± 2°C ambient temperature and 55 ± 10% humidity. All wild-type (*Fam134b*$^{+/+}$) and mutant (*Fam134b*$^{-/-}$) animals used in this study were derived by crossing founder *Fam134b*$^{+/-}$ mouse colony. Unless used for starvation experiments, all animals were fed ad libitum with standard sterile chow and water. For genotyping, tail DNA samples were extracted and subjected to PCR analysis using the following primers: Fam134b_wt_forward, 5′-ACCCCATAGTTCATACTAGGC-3′; Fam134b_mut_forward, 5′-CATGGCAATGACATTTCTCC -3′; and Fam134b_reverse, 5′-CGTAACAGAGGTTGGTGAGG-3. Product sizes of 280 bp and 420 bp represent the wild-type and mutant alleles, respectively.

Before starvation, the animals were synchronized by a prestarvation for 24 h, which is followed by free access to food for 2 h (12). After 2 h of feeding, the chow was removed from cages of starvation groups (WT-ST and KO-ST), but ad libitum (WT-AL, KO-AL) groups were allowed to access chow. Access to drinking water was free at all times. All animals were weighed at the beginning and the end of the starvation procedure. Animal age and numbers are given in the related figure legends. For the termination of experiments, the animals were euthanized using cardiac puncture-mediated exsanguination, followed by cervical dislocation under deep terminal anesthesia. Immediately after euthanasia, liver, spleen, kidney, heart, and lung tissues were collected, weighed, and snap frozen in liquid nitrogen. The whole heart tissue was used for further experimentation without compartmental dissection. The skeletal muscle tissues of mice were collected from gastrocnemius muscles. Animal and organ weight values were analyzed by the one-tailed nonparametric Mann-Whitney *U* test using the GraphPad Prism 8 software.

Bovine tissues were collected freshly from a local slaughterhouse, snap frozen in liquid nitrogen, and transferred to the laboratory under the same conditions. Bovine kidney samples were taken from kidney cortex.

Serum analyses. Whole blood was collected by cardiac puncture and immediately transferred to sterile microcentrifuge tubes with extra care to prevent hemolysis. Samples were left at room temperature for 20 min until the blood clot was formed and centrifuged for 10 min at 2,000 *g* at 4°C. Mouse serum biochemistry analyses were performed using photometric methods by an automated analyzer, Architect c16000 (Abbott) as previously shown (24, 40). Total cholesterol, high-density lipoprotein (HDL) cholesterol, and triglyceride levels were directly measured, whereas the very-low-density lipoprotein (VLDL) cholesterol levels were calculated by the triglyceride/5 formula. Low-density lipoprotein (LDL) cholesterol levels were also calculated by the

Friedewald equation: LDL = [total cholesterol − (VLDL + HDL)] (15). Serum amino acids and catabolites were analyzed by the TSQ Endura Triple Quadrupole Mass Spectrometer (Thermo Fisher Scientific) (38a). Because of insufficient serum materials, some parameters have not been tested in all experimental subjects, as indicated in related figures.

All parameters were analyzed by the one-tailed nonparametric Mann-Whitney *U* test, using the GraphPad Prism 8 software.

Plasmids. Full-length FAM134B-1 and FAM134B-2 coding sequences were obtained using PCR and cloned into p3xFLAG-CMV-10 and p3xFLAG-CMV-14 vectors using HindIII and BamHI restriction enzyme digestion sites. With the use of these vectors, coding sequences were subcloned into Tet-inducible pcDNA4TO, pEGFP-C3, and pmCherry-C2 vectors. p3xFLAG-CMV-14 and pcDNA4TO vectors contain neomycin and zeocin antibiotic selection markers, respectively.

Cell culture and generation of stable cell lines. Cells were maintained in RPMI medium supplemented with 10% fetal bovine serum, 100 IU/ml penicillin, 100 μg/ml streptomycin, and 1× nonessential amino acid (ThermoFisher). For immunofluorescence experiments, Huh7 cells were chemically transfected with mCherry-FAM134B-1 and EGFP-FAM134B-2. Cells were fixed after 24 h without further antibiotic selection. Cell lines expressing inducible FAM134B variants were generated by transfecting pcDNA4TO-FAM134B-1 and pcDNA4TO-FAM134B-2 vectors into Hep3B-TRex, a Tet repressor (pcDNA6TR) expressing cell line. FAM134B-1 and FAM134B-2 containing p3xFLAG-CMV-14 vectors were transfected into Hep3B cells. The chemical transfection of plasmids was performed using the FuGENE HD (Promega) transfection reagent. After transfection, cells were maintained under Zeocin (pcDNA4TO, 10 μg/ml) or Neomycin (p3xFLAG-CMV, 300 μg/ml) selection for 3–4 wk, and single cell-derived clones were picked, expanded, and screened by Western blot.

Antibodies. The antibodies used in Western blot were as follows: rabbit anti-FAM134B, (Sigma, HPA012077), mouse anti-FLAG (Sigma, F1804), rabbit anti-LC3B (Cell Signaling, 2775S), rabbit anti-GOPC (Cell Signaling, 8576), rabbit anti-Syntaxin 6 (Cell Signaling, 2869), rabbit anti-GM130 (Abcam, ab31561), mouse anti-58K (Abcam, ab27043), and mouse-anti Calnexin (Santa Cruz, sc23954).

Cell fractionation experiments. A fractionation experiment was performed using a slightly modified version of a previously established protocol (17). Briefly, equal amounts (5×10^6 from each) of FAM134B-1 and FAM134B-2 expressing Hep3B cell pellets were homogenized in 5 ml 0.35 M sucrose containing homogenization buffer with 50 mM Tris·HCl (pH 7.6), 25 mM KCl, 10 mM $MgCl_2$, and 2 mM DTT using a motor homogenizer (Stuart). After centrifugation at 14,000 *g*, 4°C for 10 min, the supernatant was carefully loaded on top of the discontinuous sucrose gradient, which is made up of 10 ml 1.5 M sucrose (top) and 10 ml 2 M sucrose (bottom). Samples were centrifuged at 70,000 *g*, 4°C for 16 h using SW32 Ti rotor (Beckman Coulter). By

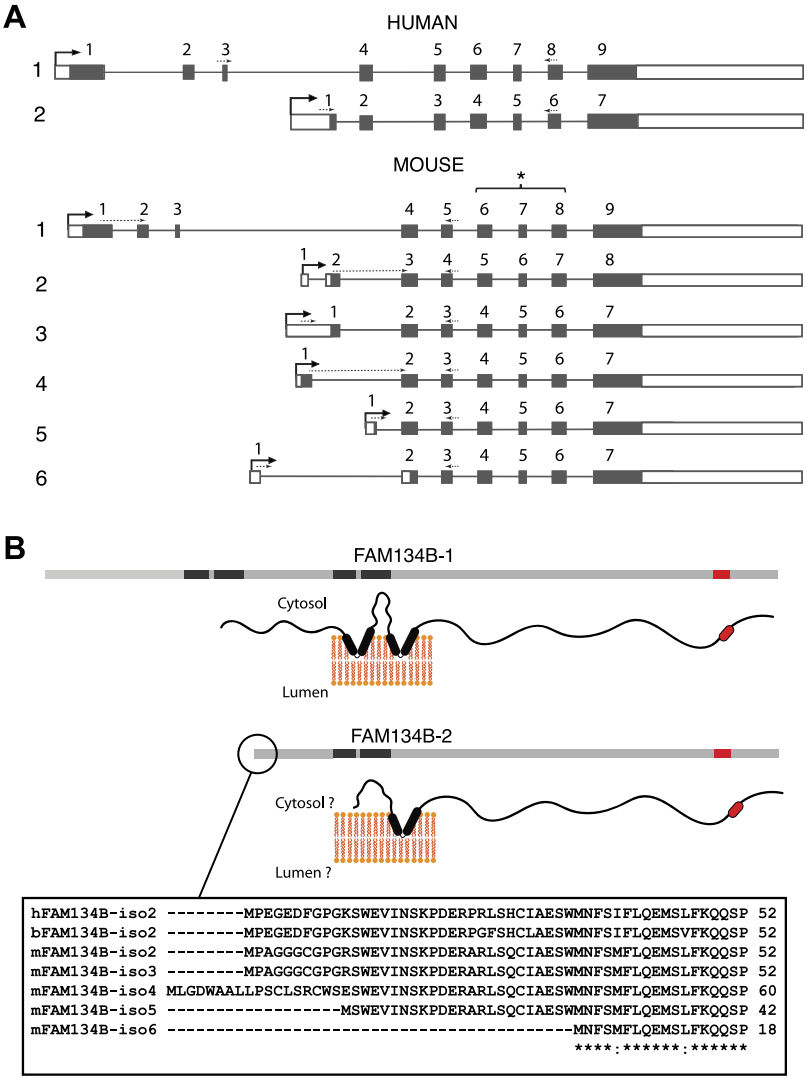

Fig. 1. Gene and protein architecture of FAM134B variants. *A*: human and mouse *FAM134B* genome organization scheme based on the National Center for Biotechnology Information reference sequencing (RefSeq) and the exon annotation based on the University of California Santa Cruz genome browser. Note that isoforms differ from each other by transcription start sites. Dashed arrows faced inwards indicate the location of selected oligonucleotides for RT-PCR. *Exons deleted for *Fam134b* knockout mouse model. *B*: schematics of human FAM134B-1 and FAM134B-2 proteins. The latter is further detailed as NH_2-terminal amino acid sequence across species in the alignment box. V-shaped black rods represent hairpin structures of transmembrane regions. Red boxes/rods indicate the LIR motif, the target of GABARAP/LC3. Prefixes h-, b- and m- represent human, bovine, and mouse *FAM134B* sequences, respectively.

puncturing the bottom of the tubes, 500-µl fractions were collected. Fraction samples were mixed with 4× Laemmli loading buffer (with 2-mercaptoethanol), making the total loading buffer concentration to 1×. Samples were directly loaded on polyacrylamide gel.

Western blot. Protein extraction from animal tissues and cell pellets were performed using RIPA lysis buffer containing 150 mM NaCl, 1% Nonidet P-40, 0.5% sodium deoxycholate, %0.1 SDS, 25 mM pH 7.4 Tris, and 1× protease inhibitor cocktail (cOmplete, Roche, 1 mM $NaOV_3$ and 1 mM NaF. Cell pellets were directly lysed in RIPA buffer, while mouse liver, pancreas, muscle, heart, testis, fat, lung, and stomach tissues were dipped in liquid nitrogen and immediately grounded into fine tissue powder with the help of a mortar and pestle. RIPA was directly added on the finely grounded tissue by taking extra care to prevent the tissue from thawing. Samples were kept on ice and vortexed every 5 min for 30 min, which was followed by centrifugation at 13,300 *g*, 4°C for 30 min. They were treated with Laemmli loading buffer containing 2-mercaptoethanol and boiled at 95°C for 3 min and were then loaded on polyacrylamide gel and run at 90 V for protein stacking and 110 V for protein resolving. Proteins were wet transferred to PVDF membrane at 400 mA for 2 h. Membranes were blocked with 5% nonfat milk powder dissolved in TBS-T [50 mM Tris·HCl (pH 7.5), 150 mM NaCl, and 0.5% Tween-20] for 1 h at room temperature. After blocking was completed, the membranes were incubated with the primary antibody diluted in blocking solution overnight at 4°C. Membranes were treated with horseradish peroxidase-conjugated secondary antibodies diluted in blocking buffer for 1 h at room temperature. After the incubation step of each antibody, membranes were washed three times with TBS-T. Protein bands were viewed using SuperSignal West Dura (ThermoFisher), and membrane images were taken via Western blot imaging system (Vilber Lourmat).

Immunofluorescence. Cells were seeded on coverslips before transfection. One day after transfection, they were fixed either with ice cold methanol (FAM134B-FLAG and 58K staining) for 20 min or 4% paraformaldehyde (EGFP and mCherry conjugated FAM134B) for 10 min at room temperature. Fixed cells transfected with FLAG tagged FAM134B were blocked with 5% BSA in PBS-T [137 mM NaCl, 2.7 mM KCl, 8 mM Na_2HPO_4, and 2 mM KH_2PO_4, (pH 7.4), 0.1% Tween-20] for 1 h at room temperature. Cells were then incubated with the primary antibody in 2% BSA overnight at 4°C. They were then incubated with anti-mouse and anti-rabbit secondary antibodies, which were conjugated with 488-nm and 594-nm fluorophores, respectively, for 1 h at room temperature. EGFP-FAM134B-2- and mCherry-FAM134B-1-transfected cells were not incubated with an antibody. Cells were stained with 100 ng/ml DAPI solution for 1 min. They were washed three times with PBS-T in between all staining procedures. Coverslips were mounted on glass slides using mounting medium (ProLong Gold Antifade Mountant, Invitrogen). Confocal images were taken using Zeiss LSM880 and processed using the ImageJ software.

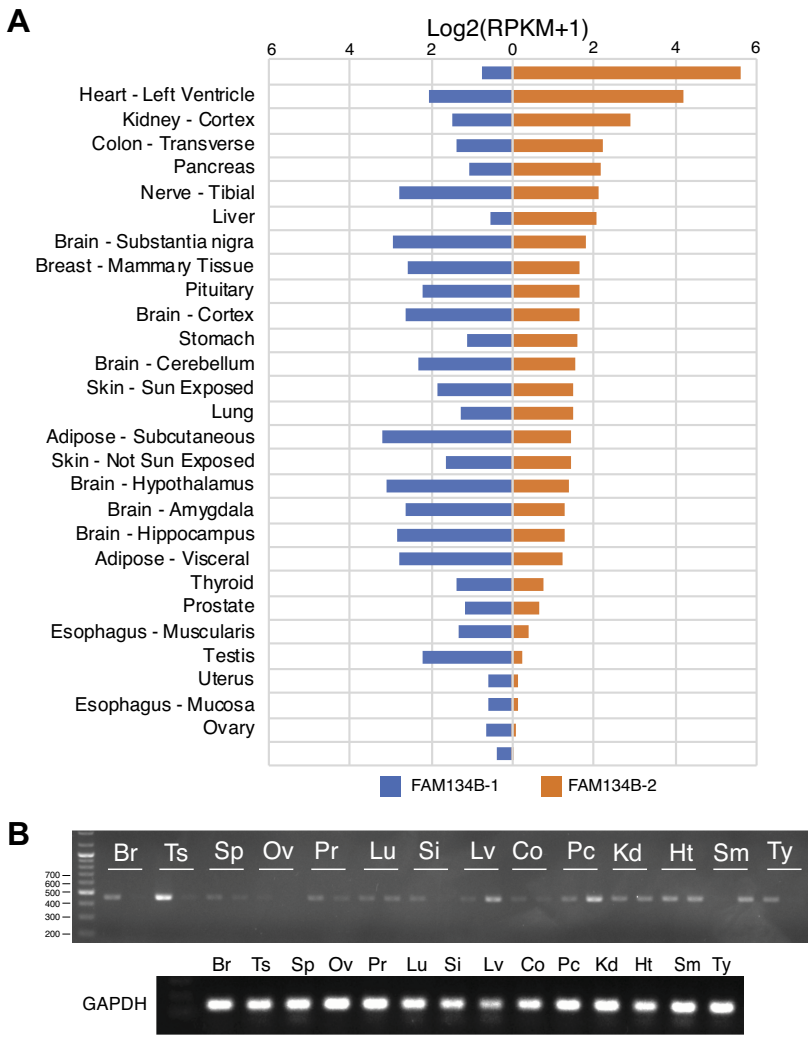

Fig. 2. *FAM134B* isoforms are differentially expressed in human tissues. *A*: GTEx RNA-sequencing data of human FAM134B isoforms represented as Log2 [mean reads per kilobase million (RPKM) + 1] (SDs are not shown). *B*: FAM134B isoform expression levels in healthy human tissue panel demonstrated by the reverse transcriptase-PCR (RT-PCR). Equal loading control PCR performed by using GAPDH primers. The tissue name coding is as follows: Br, brain; Ts, testis; Sp, spleen; Ov, ovaries; Pr, prostate; Si, small intestine; Lv, liver; Co, colon; Pc, pancreas; K_d, kidney; Ht, heart; Sm, skeletal muscle; Ty, thymus. For each tissue, FAM134B-1 and FAM134B-2 bands were loaded at left- and right-hand side, respectively. Predicted band sizes according to in silico PCR is as follows: FAM134B-1, 450 bp; FAM134B-2, 449 bp.

RESULTS

Genomic organization of FAM134B and its protein isoforms. The human *FAM134B* gene is located on chromosome 5p and spans a 144-kb region. The structural organization of the human and mouse full-length orthologs is quite similar, with nine exons and eight introns. Two transcript isoforms, namely *FAM134B-1* and *FAM134B-2*, are generated from the human (Fig. 1*A*, *top*) and bovine (not shown) genes, while the mouse gene serves as a template to generate six isoforms (Fig. 1*A*, *bottom*). The *FAM134B-1* isoform is generated by transcriptional initiation from the DNA sequence 5′ of exon 1, whereas other isoforms have alternative start sites all located in intron 3 in both human and mouse (Fig. 1*A*). The translation of these transcripts generates a full-length FAM134B-1 protein isoform and an NH_2 terminally truncated FAM134B-2 protein isoform in both human and bovine species. The mouse also generates a *FAM134B-1* isoform, as well as several NH_2 terminally truncated isoforms (all short forms are referred to as *FAM134B-2* in this report for simplicity).

The domain organization of the full-length FAM134B-1 is characterized by a hydrophilic NH_2-terminal domain, followed by the hydrophobic RHD that spans the cytoplasmic leaflet of the ER membrane, and a hydrophilic COOH-terminal domain. The RHD of FAM134B is composed of two transmembrane domains, namely TM12 and TM34, which are separated by a hydrophilic loop facing the cytoplasm (6, 22). On the other hand, NH_2 terminally truncated FAM134B-2 protein isoforms are composed of a short hydrophilic NH_2-terminal domain, followed by the single hydrophobic TM34 domain of the RHD, and completed by an intact hydrophilic COOH-terminal domain (Fig. 1*B*). Both short and long isoforms harbor a LIR motif located near the end of the hydrophilic COOH-terminal domain (Fig. 1*B*).

FAM134B isoforms are differentially expressed in normal adult tissues. The localization of transcription start sites of all short isoforms within intron 3 of the *FAM134B* gene strongly suggested that the expression of long and short *FAM134B* transcript isoforms are controlled by different factors and/or mechanisms. This led us to compare the tissue-specific expression of full-length and truncated *FAM134B* isoforms. First, we analyzed normal tissue expression data on human isoforms available at the GTEx database (3). We observed striking differences between tissues in terms of *FAM134B* gene expression (Fig. 2*A*).

FAM134B-1 is strongly expressed in the brain, which also expresses *FAM134B-2* at lower levels. A stronger expression of *FAM134B-1* was also seen in the tibial nerve, adipose tissue and testis. Many other tissues including the skeletal muscle, heart, kidney cortex, colon, pancreas, liver, and stomach displayed a strong expression of *FAM134B-2* compared with *FAM134B-1*. A few tissues such as the uterus and ovary were observed to

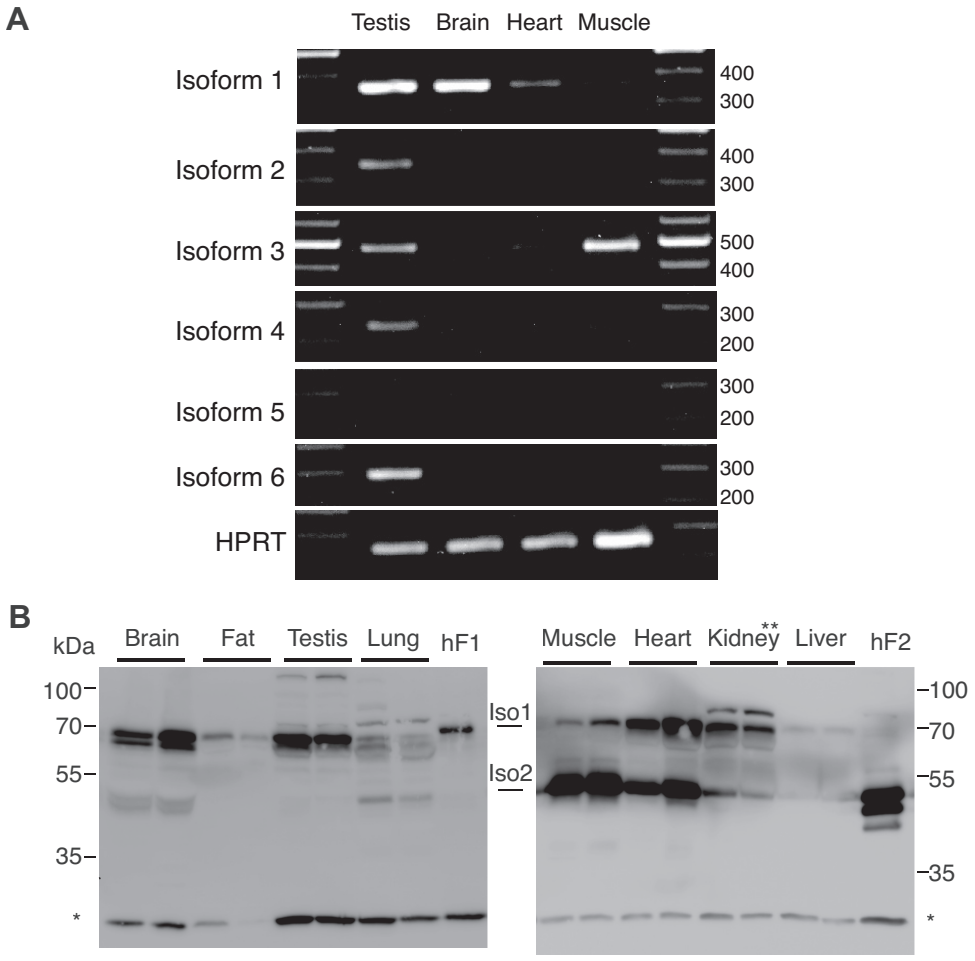

Fig. 3. FAM134B isoforms are differentially expressed in mouse and bovine tissues. *A*: differentially expressed *Fam134b* variants in mouse testis, brain, heart, and skeletal muscle, shown by RT-PCR. *B*: Western blot results of bovine brain, fat, testis, lung, skeletal muscle, heart, kidney, and liver probed by FAM134B antibody. hF1 and hF2 lanes represent positive control protein lysates of Hep3B cell line stably expressing human FAM134B-1 and FAM134B-2, respectively. *Nonspecific antibody binding; **kidney samples were taken from kidney cortex.

have a weak expression of both *FAM134B* isoforms (Fig. 2*A*). We strived to confirm the differential expression of *FAM134B* isoforms by an RT-PCR analysis of a panel of 14 human tissues. As shown in Fig. 2*B*, experimental data confirmed the differential expression of *FAM134B-1* and *FAM134B-2* transcripts in these tissues. For example, the brain, testis, spleen, and prostate were rich in *FAM134B-1* expression. In contrast, the skeletal muscle, pancreas, and liver displayed a stronger expression of *FAM134B-2*. As expected, no significant signal was observed in the ovarian tissue.

We also analyzed the expression patterns of *Fam134b* transcripts in several mouse tissues. As shown in Fig. 3*A*, mouse testis strongly expressed all isoforms except for isoform-5. The mouse brain showed a strong expression of isoform-1 with a

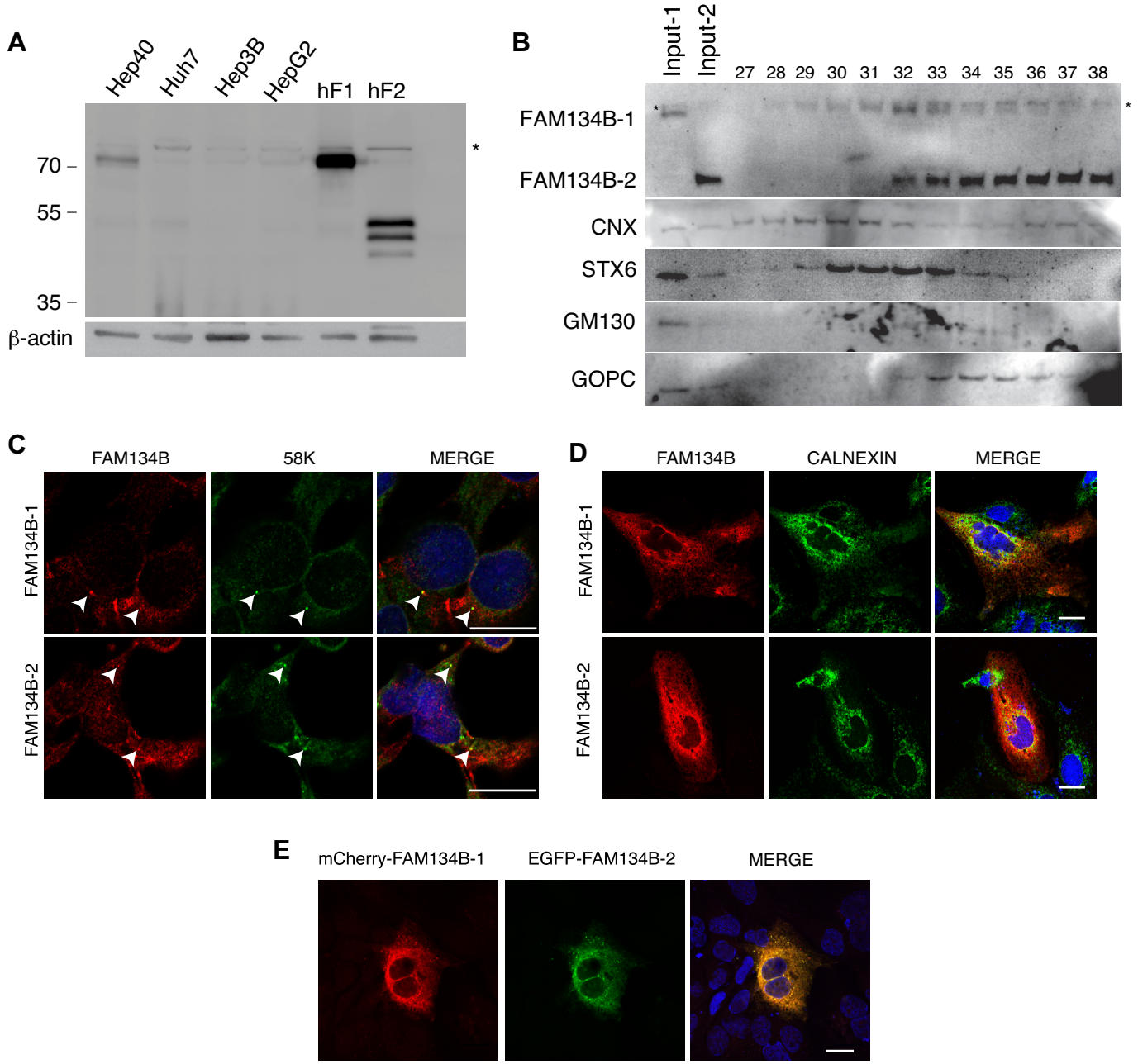

Fig. 4. FAM134B isoforms are weakly expressed endogenously in cell lines and differentially localize in subcellular compartments. *A*: Western blot result showing the basal levels of FAM134B in well-differentiated HCC cell lines. *Nonspecific antibody binding. hF1 and hF2 shows stable FAM134B-1 and FAM134B-2 expressions in Hep3B cell line, respectively. *B*: sucrose gradient fractionation of Hep3B cells stably expressing FAM134B-1-FLAG and FAM134B-2-FLAG vectors. The numbers above the picture, from *left* to *right*, represent the heavier to lighter fractions. FAM134B is probed by anti-FAM134B antibody. Calnexin (CNX) is used as endoplasmic reticulum (ER) marker; GOPC, GM130, and STX6 are used as Golgi markers. Note that specific FAM134B-1 bands reach a peak at fraction 32 and decrease thereafter. However, protein bands from nonspecific antibody binding, marked with asterisk, start from fraction 31 and increase in following lighter fractions. *C*: partial colocalization of Golgi marker 58K with both FAM134B-1 and FAM134B-2. White arrowheads show FAM134B- and 58K-positive punctae. *D*: immunofluorescence imaging of FAM134B isoforms and ER resident protein Calnexin. *E*: immunofluorescence imaging of mCherry-FAM134B-1 and EGFP-FAM134B-2, coexpressed in Huh7 cell line. Scale bars in *C*, *D*, and *E* = 20 μm.

weak expression of isoform-2, -4, and -6. The heart was weakly positive for isoform-1, -3, -4, -5, and -6. The muscle stood apart by a strong expression of isoform-3, together with a weak expression of isoform-1, -2, and -4.

Differential expression of FAM134B protein isoforms in normal tissues. A further verification of *FAM134B* isoform expression in different tissues was performed at protein level by Western blotting. We initially applied Western blotting experiments to bovine species, which express only two transcript isoforms, similar to human, as stated above. As shown in Fig. 3*B*, bovine FAM134B-1 and FAM134B-2 proteins migrated with apparent molecular weights of 70 kDa and 50 kDa, respectively, similar to human isoforms. The dominant expression of FAM134B-1 was observed in the brain, adipose, testis, and kidney, while FAM134B-2 was dominant in the heart and muscle. The weak expression of both isoforms was detected in the lung tissue. The bovine liver stood apart by little to no expression of both FAM134B protein isoforms.

FAM134B isoforms differentially localize in subcellular compartments. FAM134B has previously been identified as an ER and Golgi-associated protein (22, 25). As the studied isoform(s) has not been specified in these studies, we went on to compare the two isoforms for their subcellular localization. Initial analysis of four well-differentiated (16, 44) liver cancer cell lines failed to detect FAM134B isoforms in these cell lines, except for the Hep40 displaying a weak FAM134B-1 expression (Fig. 4*A*). We constructed Hep3B-derived cells stably expressing FLAG-tagged FAM134B-1 or FAM134B-2.

To investigate the subcellular localization of both isoforms in the same experiment, we performed cell fractionation studies followed by Western blot analysis. We first prepared cell extracts (Fig. 4*B*, lines input-1 and input-2, respectively) before a sucrose gradient. Sucrose fractions were then collected from the bottom of the gradient making tube and subjected to Western blotting using antibodies for FAM134B, as well as Golgi markers GOPC (9), GM130 (30), and STX6 (34) and CNX (ER, but leaky; Ref. 33).

FAM134B-2 colocalized with GOPC and cis-Golgi marker GM130 but not with trans-Golgi marker STX6 fractions, while calnexin was expanded to many fractions and colocalized with both isoforms. On the other hand, both FAM134B isoforms partially colocalized with Golgi marker 58K (4), demonstrated by immunofluorescent staining (Fig. 4*C*). Immunofluorescence analysis of FAM134B-1 and FAM134B-2 indicated that when ectopically expressed, they mostly colocalize with each other, and they also colocalize with Calnexin (Fig. 4, *D* and *E*), suggesting ER-localization.

Starvation increases FAM134B-2 RNA and protein in the liver. As *FAM134B* is involved in ER-phagy during starvation (22), we studied its expressional changes in mice following starvation. Wild-type and *Fam134b*$^{-/-}$ mice were either fed ad libitum or starved up to 48 h, followed by an expression analysis of *FAM134B* isoforms. Tissues obtained from *Fam134b*$^{-/-}$ mice were used as negative controls. Our FAM134B antibody cross reacted with several nonspecific proteins in mouse tissues, thus limiting our analysis to only the FAM134B-2 isoform (Fig. 5, *A*, *C*, and *D*).

We first analyzed LC3B and FAM134B-2 expression in the liver after 48 h of starvation. Autophagy induction in the liver as a response to starvation was shown by a decrease in p62 protein levels and induced levels of autophagosome-associated LC3B-II and LC3B-I (Fig. 5*A*). We also noticed that LC3B-I levels were more pronounced in *Fam134b*$^{-/-}$ mice compared with wild-type mice (Supplemental Fig. S1; all Supplemental material available at https://figshare.com/articles/figure/Suppl_Keles_et_al_30_03_2020_pdf/12047520). FAM134B-2 was not detected in *Fam134b*$^{-/-}$ mice, as expected. *Fam134b*$^{+/+}$ and *Fam134b*$^{+/-}$ mice showed an induced expression after starvation at 50 kDa (Fig. 5*A* and Supplemental Fig. S1). In addition to the 50-kDa FAM134B-2, a specific smaller 35-kDa protein was also induced in wild-type animals (Fig. 5*A*, marked with a single asterisk). Additional starvation experiments performed

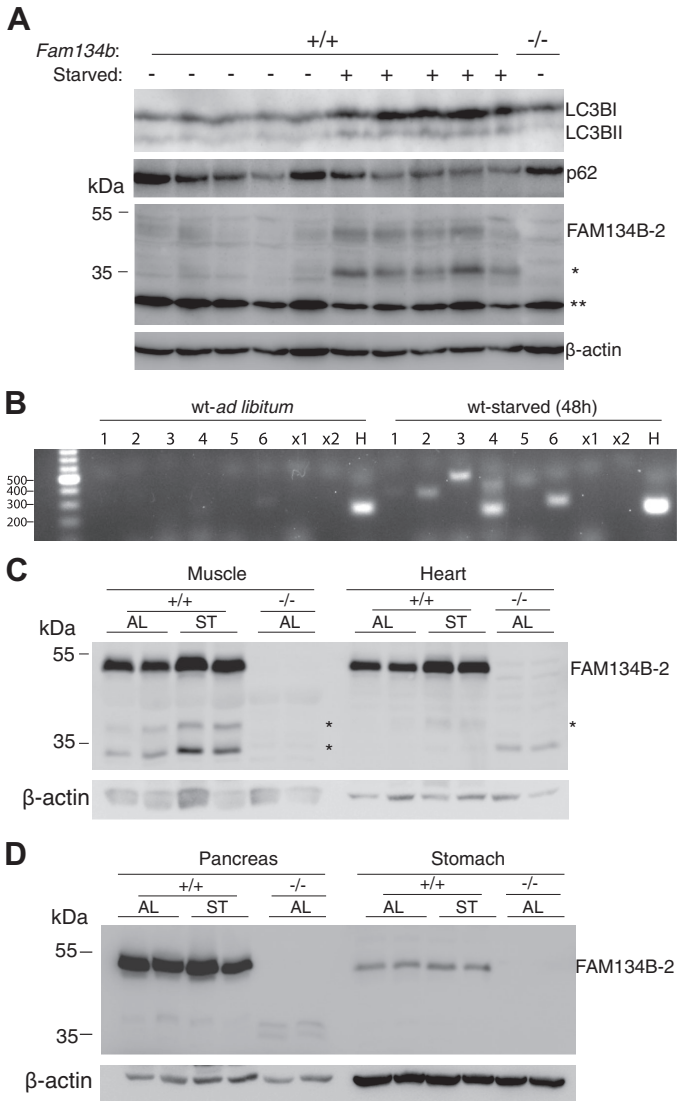

Fig. 5. Starvation induces *FAM134B-2* in liver, muscle, and heart in mice. *A*: protein levels of FAM134B-2, p62, and LC3B in livers of mutant and wild-type mice (12-wk-old, male) upon 48-h starvation. *FAM134B-2 is observed near 55 kDa, along with the additional band at 35 kDa. **Nonspecific antibody binding. *B*: mRNA levels of *Fam134b* isoforms in 48-h starved mouse liver. Numbers indicate the mouse *Fam134b* variants; H, mouse HPRT. Expected band sizes according to in silico PCR are as follows: isoform-1, 354 bp; isoform-2, 343 bp; isoform-3, 474 bp; isoform-4, 231 bp; isoform-5, 256 bp; isoform-6, 286 bp; isoform X1, 469 bp; isoform X2, 473 bp. *C* and *D*: tissue-specific changes in FAM134B-2 levels upon 36-h starvation (18-mo-old mice, male) are demonstrated for skeletal muscle (gastrocnemius) and heart (*C*) and for pancreas and stomach (*D*).

for 24 h have exhibited an even stronger stimulation than of 48 h (Supplemental Fig. S2).

To test whether FAM134B protein accumulation in starved animal liver was associated with transcriptional upregulation, we performed an RT-PCR analysis of six mouse isoforms along with two additional putative protein coding transcripts, X1 and X2. The starvation induced the expression of isoform-3, -4, and -6 strongly and isoform-2 weakly, while the level of isoform-5 was not changed. There was little to no expression of isoform-1 in both fed and starved conditions (Fig. 5*B*). There was also no induced expression of putative transcripts X1 and X2.

Starvation increases FAM134B-2 in the muscle and heart. To observe possible starvation induced FAM134B-2 response in other organs, we expanded our analysis with mouse heart, muscle, pancreas, and stomach. Similar to the liver, FAM134B-2 protein levels as well as shorter protein fragments near 35 kDa in the muscle and heart were elevated following starvation (Fig. 5*C*). Stimulation of autophagy was confirmed by increased shift from LC3B-I to LC3B-II (Supplemental Fig. S3). Under the same conditions, there was no change in FAM134B-2 levels in the pancreas or stomach (Fig. 5*D*).

Upon starvation, Fam134b$^{-/-}$ mice display less weight loss and increased serum albumin levels along with disrupted amino acid release. To analyze the in vivo response of *Fam134b*-deficient tissues to starvation, we compared *Fam134b*$^{+/+}$ and *Fam134b*$^{-/-}$ mice for their response to nutrient starvation for 36 h. The initial body weights of tested animals were similar with no significant differences (n = 73) (Supplemental Fig. S4). Starvation induced significant whole body and tissue-specific weight loss in both wild-type and *Fam134b*$^{-/-}$ mice (Fig. 6). Among the tissues analyzed, there was significant weight loss in the liver, kidney, spleen, and heart for both wild-type and mutant animals, and significant loss of lung weight was observed only in mutant animals. Interestingly, starved mutant animals slightly resisted body weight loss compared with wild-type mice, as shown by body weight change as percentage (Fig. 6, body weight change).

Autophagic proteolysis in the liver following starvation makes a significant contribution to the maintenance of blood glucose levels via conversion of amino acids to glucose, and accordingly, many amino acids are released into the blood by 24 h of starvation (12). Therefore, we measured serum glucose and amino acid levels in both wild-type and *Fam134b*$^{-/-}$ mice after 36 h of starvation. There was a significant decrease in serum glucose in both wild type and mutant mice, the fall in *Fam134b*$^{-/-}$ being more significant (Fig. 7*A*). Wild-type animals displayed a significant increase in serum levels of amino acids glutamine, asparagine, alanine, serine, glycine, tryptophan, threonine, and lysine. *Fam134b*$^{-/-}$ mice failed to increase the levels of these amino acids with the exception of threonine (Fig. 7*B*). There was no change in the levels of histidine, proline, valine, methionine, and tyrosine in wild-type mice,

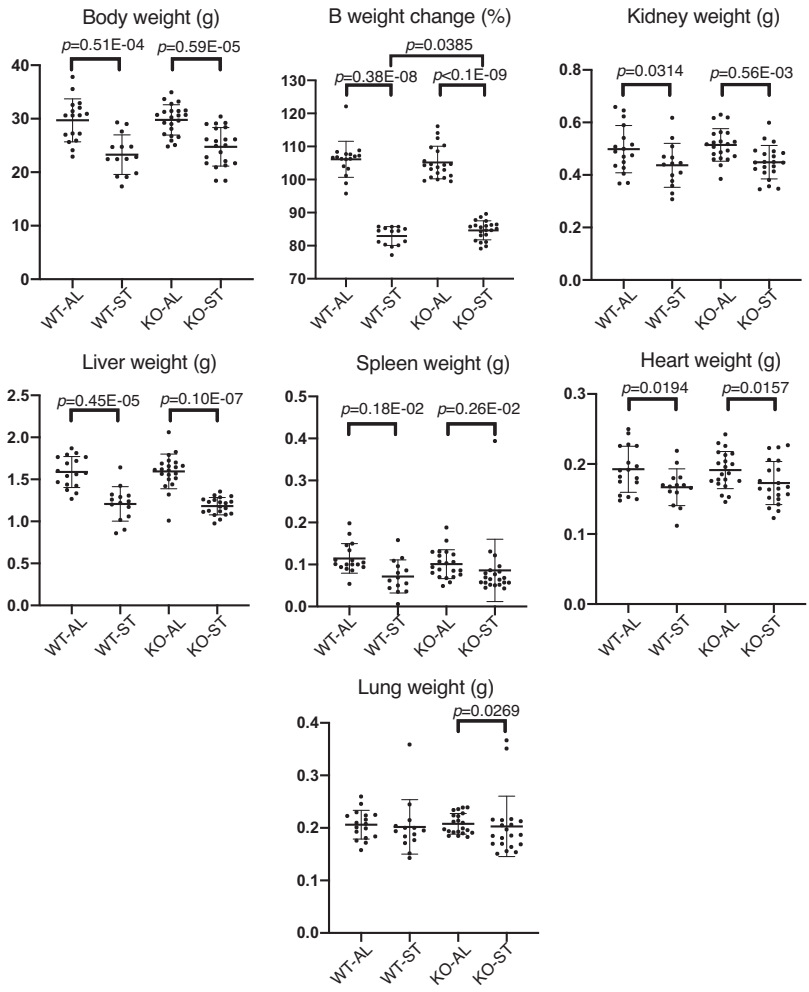

Fig. 6. Upon starvation for 36 h, *Fam134b*$^{-/-}$ mice displayed resistance to total body weight loss. Eighteen-month-old mice (n = 73) were used for body and organ weight calculation with following groups: *Fam134b*$^{+/+}$-ad libitum (WT-AL), n = 17 (9 male, 8 female); *Fam134b*$^{+/+}$ starvation (WT-ST), n = 14 (8 male, 6 female); *Fam134b*$^{-/-}$-ad libitum (KO-AL), n = 21 (13 male, 8 female); *Fam134b*$^{-/-}$- starvation (KO-ST), n = 21 (13 male, 8 female). Mann-Whitney nonparametric test results are represented as means ± SD. $P < 0.05$ was considered as significant. Nonsignificant results are not indicated.

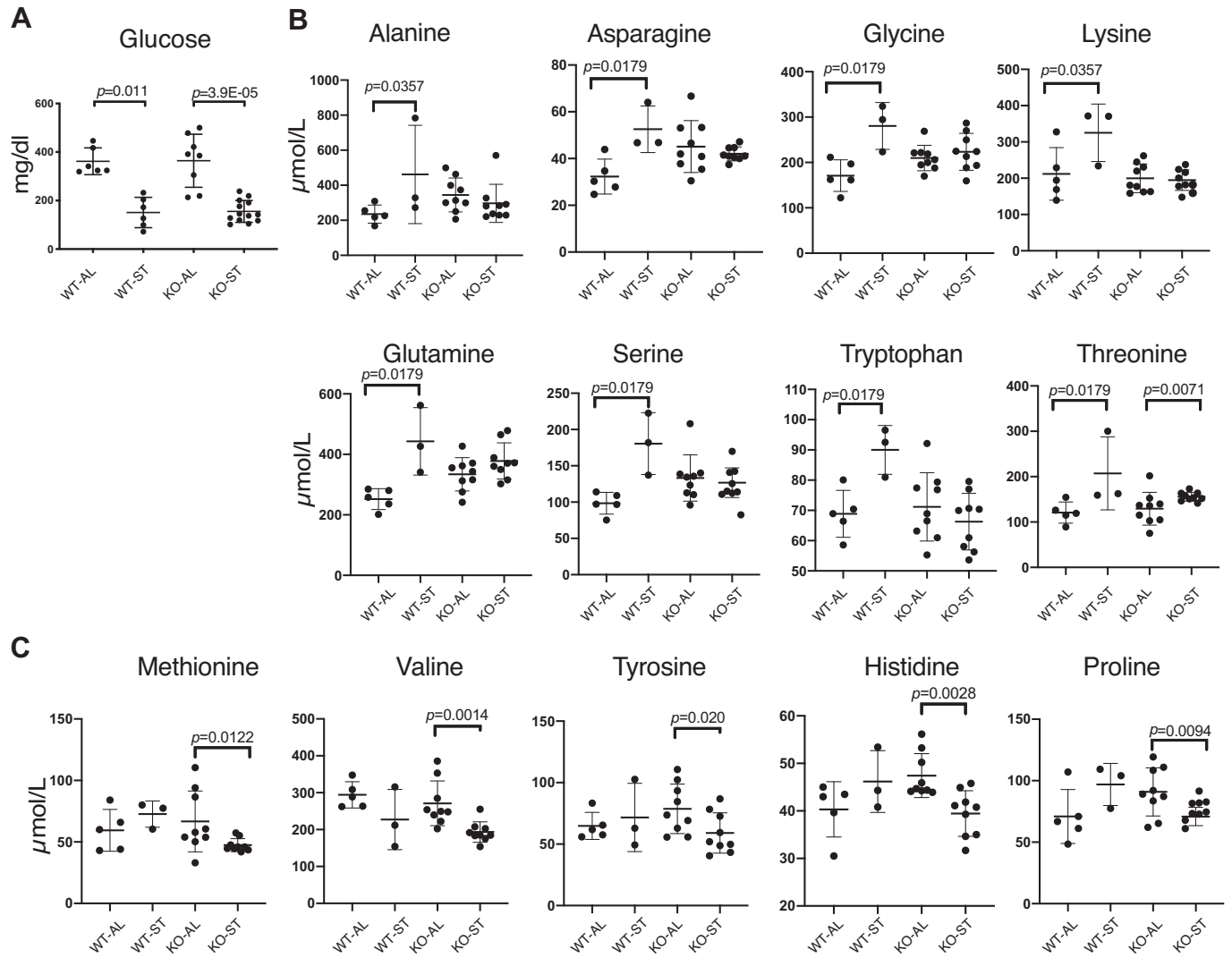

Fig. 7. Amino acid release into blood following 36 h of starvation is aberrant in *Fam134b*$^{-/-}$ mice. *A*: serum glucose levels. *B*: serum amino acids with increased levels in wild-type but not in *Fam134b*$^{-/-}$ mice. *C*: serum amino acids with decreased levels in *Fam134b*$^{-/-}$ but not in wild-type mice. Because of insufficient amount of serum some samples were unavailable for amino acid analyses. The animals included in amino acid analyses were an average of 18 mo old, and the animal groups were as follows: *Fam134b*$^{+/+}$-ad libitum (WT-AL), $n = 5$ (4 male, 1 female); *Fam134b*$^{+/+}$-starvation (WT-ST), $n = 3$ (2 male, 1 female); *Fam134b*$^{-/-}$-ad libitum (KO-AL), $n = 9$ (6 male, 3 female); *Fam134b*$^{-/-}$-starvation (KO-ST), $n = 9$ (8 male, 1 female) Mann-Whitney nonparametric test results are represented as means ± SD. $P < 0.05$ was considered as significant. Nonsignificant results are not indicated.

but interestingly, all these five amino acids underwent a significant drop in *Fam134b*$^{-/-}$ mice (Fig. 7*C*).

Other changes in starved Fam134b$^{-/-}$ *mice.* We further investigated the *Fam134b* associated phenotype by analyzing serum levels of proteins, nutrients, electrolytes and enzymes. Interestingly, baseline high-density lipoprotein (HDL) cholesterol levels were significantly lower in mutant animals. Starvation induced a decrease in serum levels of triglycerides, very-low-density lipoprotein (VLDL), and low-density lipoprotein (LDL) cholesterol but not in total cholesterol in either group of animals (Fig. 8).

Starvation also induced serum levels of albumin and total protein in *Fam134b*$^{-/-}$ but not in wild-type mice (Fig. 8). Wild-type animals showed elevated levels of blood urea nitrogen, as reported previously (41), but no such significant change was observed in mutant mice.

Changes in serum ions such as sodium, potassium, chloride, calcium, and iron were also observed (Fig. 9). Upon starvation, sodium, potassium, and chloride displayed significant increases in both wild-type and *Fam134b*$^{-/-}$ mice. In contrast, calcium levels in wild-type animals and iron levels in both groups were decreased. The lack of starvation-induced hypocalcemia in *Fam134b*$^{-/-}$ mice was noteworthy.

Finally, starvation resulted in liver injury as evidenced by increased levels of serum AST and ALT in both groups of animals. Of particular interest, serum α-amylase activity was significantly upregulated in *Fam134b*$^{-/-}$ but not in wild-type mice (Fig. 10), suggesting starvation-induced pancreas injury.

Expression of FAM134B isoforms is suppressed or stimulated in different cancers. As stated earlier, the expression changes of *FAM134B* have been described in esophageal, colon, breast, and liver cancers (9–14). Our observations described so

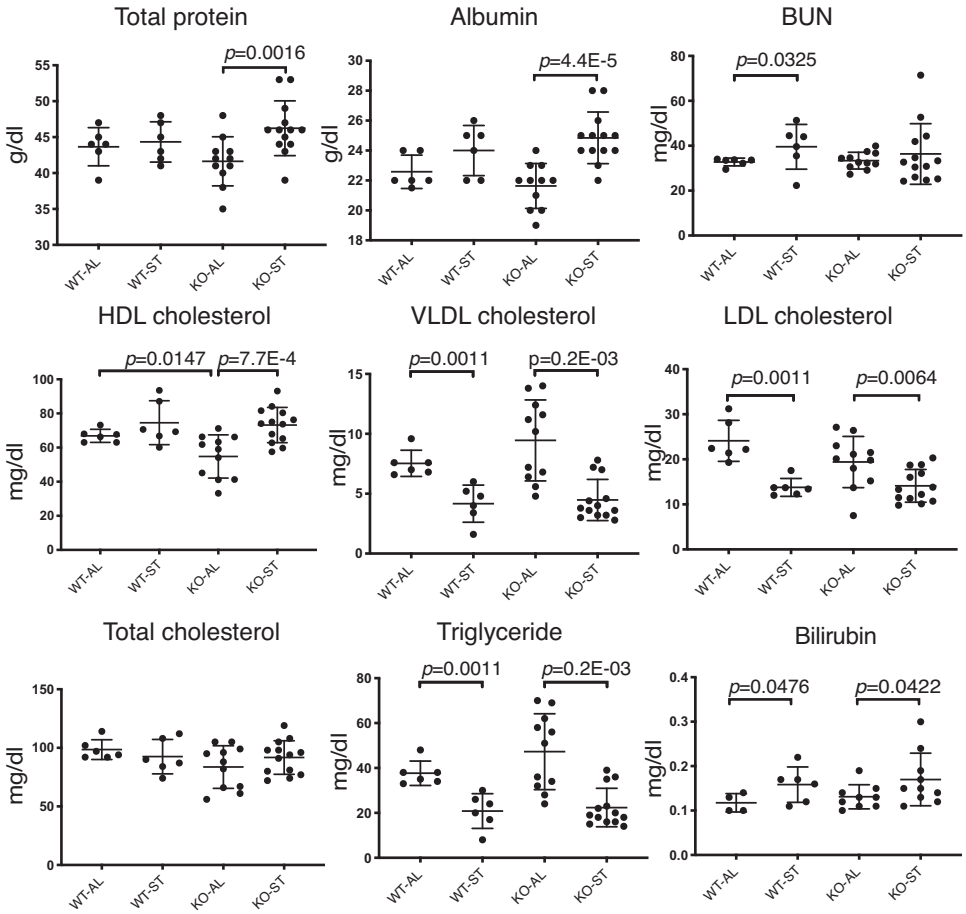

Fig. 8. Upon 36-h starvation, *Fam134b*$^{-/-}$ mice displayed a significant increase in serum albumin and total serum protein levels, but there was no major difference from wild-type animals in urea, lipoproteins, lipids and bilirubin levels. The animals tested for serum biochemistry were an average of 18 mo old, and the groups were as follows: *Fam134b*$^{+/+}$-ad libitum (WT-AL), n = 6 (4 male, 2 female); *Fam134b*$^{+/+}$ starvation (WT-ST), n = 6 (4 male, 2 female); *Fam134b*$^{-/-}$-ad libitum (KO-AL), n = 11 (8 male, 3 female); *Fam134b*$^{-/-}$-starvation (KO-ST), n = 13, (9 male, 4 female). BUN, blood urea nitrogen; VLDL, very-low-density lipoprotein; LDL, low-density lipoprotein; HDL, high-density lipoprotein. Mann-Whitney nonparametric test results are represented as means ± SD. $P < 0.05$ was considered as significant. Nonsignificant results are not indicated.

far show that the human *FAM134B* gene encodes at least two different protein isoforms: one full-length with an intact RHD domain (i.e., FAM134B-1) and an NH_2 terminally truncated form with a disrupted RHD domain (i.e., FAM134B-2). Previously published data on FAM134B in cancers did not specify what type of FAM134B protein is implicated in different cancers. To clarify this issue, we collected following data sets from the TSVdb database: hepatocellular carcinoma (371 tumors and 50 nontumor liver), lung adenocarcinoma (515 tumors and 59 normal), lung squamous carcinoma (501 tumors and 51 normal), colon adenocarcinoma (285 tumors and 41 normal), stomach adenocarcinoma (415 tumors and 35 normal), and kidney chromophobe cancer (66 tumors and 25 normal), and we performed an isoform level differential expression analysis on these publicly available transcriptome data.

As shown in Fig. 11, both *FAM134B-1* and *FAM134B-2* isoforms were positive in nontumor colon, lung, (Fig. 11*A*), stomach, and kidney (Fig. 11*B*) tissues. In contrast, only *FAM134B-2* was positive with a marginal expression of *FAM134B-1* in nontumor liver samples (Fig. 11*A*). HCC samples displayed a significant downregulation of *FAM134B-2* (Fig. 11*A*). We confirmed this finding by performing an RT-PCR analysis on HCC tumors (n = 11) and nontumor liver tissues (n = 16), which showed a loss of the *FAM134B-2* signal in most HCC tumors analyzed (Fig. 11*C*).

A significant downregulation of both *FAM134B-1* and *FAM134B-2* was observed in colon and lung cancers (Fig. 11*A*). In contrast, FAM134B-2 was significantly upregulated in stomach adenocarcinoma. Finally, both FAM134B-1 and FAM134B-2 were significantly upregulated in chromophobe renal cell carcinomas (KICH). Other tumors including breast and prostate cancer did not display significant changes in the *FAM134B* isoform expression (not shown).

DISCUSSION

We performed a comprehensive analysis of the *FAM134B* gene, its transcripts, and encoded protein isoforms together with its implications in nutrient starvation and cancer. Our main findings indicate that human and bovine species express at least two different transcript isoforms encoding a full-length and an NH_2 terminally truncated protein isoform. In contrast, mice encode at least six different transcript isoforms, giving rise to one full-length and five NH_2 terminally truncated proteins. During the preparation of this report for publication, we became aware of a publication by Kohno et al. (23) on the identification of a novel *FAM134B-2* transcript isoform capable of encoding an NH_2 terminally truncated protein in the livers of fasted mice. This transcript may represent either isoform-2 or isoform-3 described in our report (Fig. 1). In addition to isoform-2 and -3, mouse tissues exhibited the expression of isoform-4, -5, and -6, all capable of encoding four different NH_2 terminally truncated proteins that differ from each other at the first 45 amino acids of the NH_2-terminal region (Fig. 1*B*).

The FAM134B-2 protein lacks the NH_2-terminal tail and the TM12 reticulon structure of the full-length protein but retains

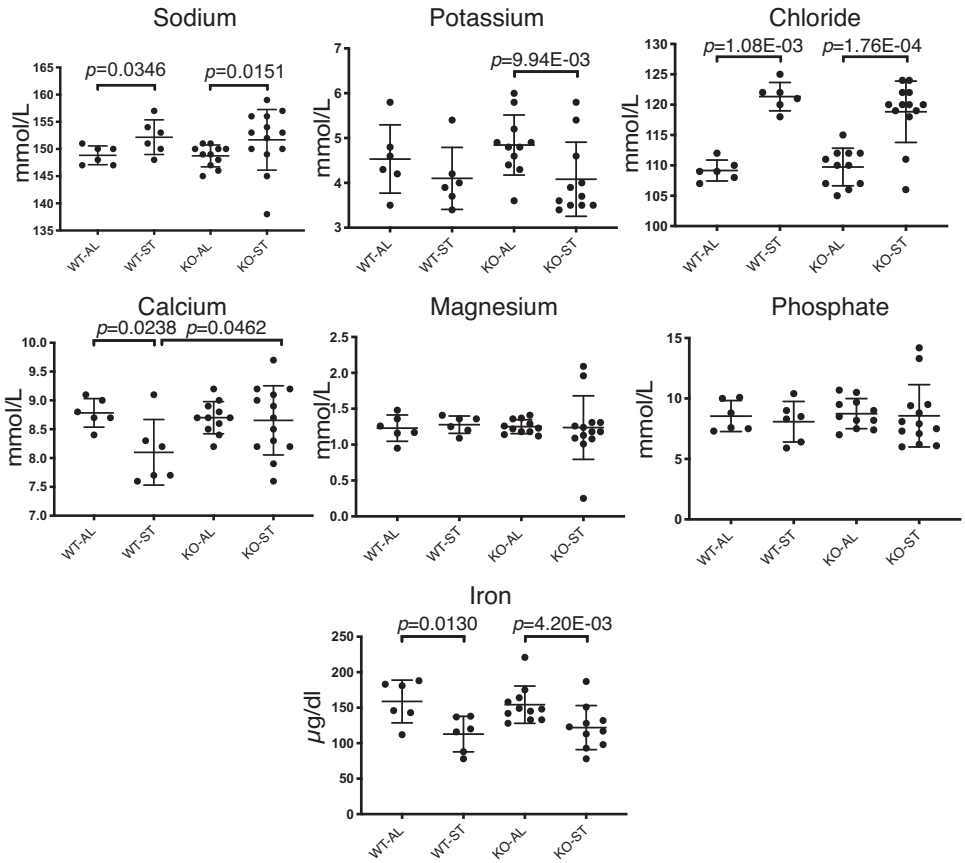

Fig. 9. Upon 36-h starvation, *Fam134b*$^{-/-}$ mice avoided starvation induced hypocalcemia as tested by serum calcium levels. The animals tested for serum electrolyte levels were an average of 18 mo old, and the groups were as follows: *Fam134b*$^{+/+}$-ad libitum (WT-AL), $n = 6$ (4 male, 2 female); *Fam134b*$^{+/+}$-starvation (WT-ST), $n = 6$ (4 male, 2 female); *Fam134b*$^{-/-}$-ad libitum (KO-AL), $n = 11$ (8 male, 3 female); *Fam134b*$^{-/-}$-starvation (KO-ST), $n = 13$, (9 male, 4 female). Mann-Whitney nonparametric test results are represented as means ± SD. $P < 0.05$ was considered as significant. Nonsignificant results are not indicated.

the TM34 reticulon along with the COOH-terminal region, which harbors the LC3B binding LIR motif. It was previously shown that the remaining reticulon structure, namely TM34, is critical for membrane shaping (6) and that the LIR motif of FAM134B-2 still mediates ER-phagy (23). However, FAM134B-2 is unlikely to be a mere compensatory protein for FAM134B-1, since FAM134B-1 cleavage by the zika virus yields a truncated protein very similar to FAM134B-2 that is unable to promote reticulophagy (26).

Our subcellular localization studies with human FAM134B-1 and human FAM134B-2 indicated that loss of integrity of the RHD in the shorter isoform did not abolish the ability of FAM134B-2 to localize to the ER (Fig. 4, *B* and *D*). However, the two isoforms of FAM134B did not completely colocalize, as shown in Fig. 4*B*. Colocalization of FAM134B-2 with the Golgi marker GOPC, GM130 (Fig. 4*B*), and 58K (Fig. 4*C*) but not with STX6 strongly suggested that this form may be preferentially localized at the ER membrane close to the Golgi apparatus. Indeed, mouse liver FAM134B-2 was shown to be localized at both the rough and smooth ER (23).

To detail the physiological relevance of *FAM134B* variants, we analyzed their distribution in human, bovine, and mouse tissues. One of our most striking findings is the identification of the *FAM134B-2* transcript as the dominantly expressed form in the skeletal muscle, heart, kidney cortex, colon, pancreas, liver, and stomach. This contrasts sharply with the dominant expression of *FAM134B-1* in the brain, tibial nerve, adipose tissue, and testis. Our Western blot analyses with bovine and mouse tissues have further shown that the tissue-specific expression of FAM134B is conserved during evolution (Figs. 3 and 5). This may indicate that *FAM134B-1* and *FAM134B-2* are involved in some tissue-restricted functions. For example, *FAM134B-2* may be involved in the lysosomal degradation of a subgroup of ER components rather than bulk ER degradation (or turnover), which was previously elaborated for the liver (23). As the FAM134B-2 protein is distinctly colocalized to ER and Golgi, it may have a role during the transfer of protein and lipid molecules from ER to Golgi or in autophagy-related changes during the trafficking, processing, and sorting of the newly synthesized membrane and secretory proteins and lipids.

Reticulon-homology domain (RHD)-containing proteins are well known as ER-shaping elements, and their deficiency results in a disturbed ER network (10). Furthermore, proteins harboring a single transmembrane structure (e.g., TM12 or TM34 alone) were previously shown to be involved in shaping ER tubules (46). Despite carrying a truncated RHD, a pronounced expression of FAM134B-2 in the muscle and heart might indicate a similar structural role in ER shaping and organization. However, besides the previously identified sensory neuropathy, no major phenotype has been observed even in aged animals, indicating that *Fam134b* deficiency is well tolerated, possibly due to a compensatory mechanism that is yet to be understood.

From simple prokaryotes to humans, all living organisms are equipped with complex survival mechanisms to cope with nutrient scarcity. Starvation initiates a cascade of events including autophagy, thereby mobilizing energy sources to meet the energy demands of vital organs. In this complex mechanism, the liver, heart, skeletal muscle, and kidney play critical roles in regulating the release and uptake of major energy sources such

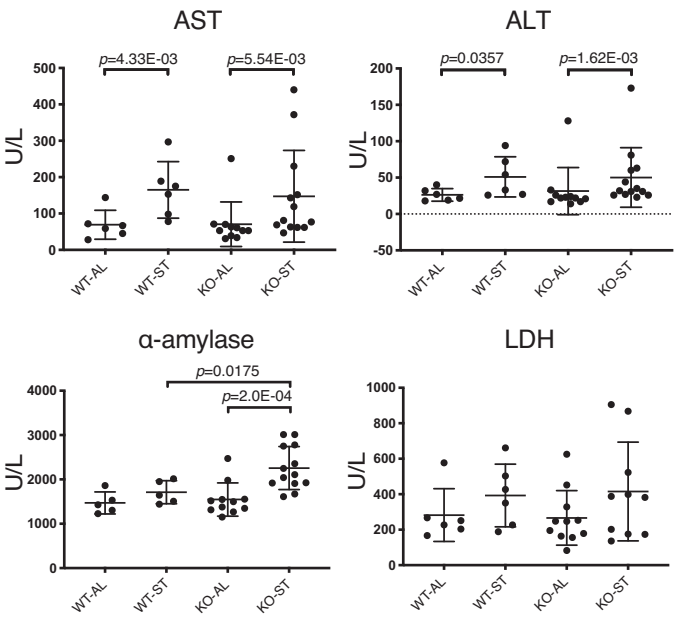

Fig. 10. *Fam134b*$^{-/-}$ mice have an elevated serum α-amylase after 36-h starvation. The animals tested for serum enzyme levels were an average of 18 mo old, and the groups were as follows: *Fam134b*$^{+/+}$-ad libitum (WT-AL), n = 6 (4 male, 2 female); *Fam134b*$^{+/+}$-starvation (WT-ST), n = 6 (4 male, 2 female); *Fam134b*$^{-/-}$-ad libitum (KO-AL), n = 11 (8 male, 3 female); *Fam134b*$^{-/-}$-starvation (KO-ST), n = 13, (9 male, 4 female). AST, aspartate aminotransferase; ALT, alanine aminotransferase; LDH, lactate dehydrogenase. Mann-Whitney nonparametric test results are represented as means ± SD. $P < 0.05$ was considered as significant. Nonsignificant results are not indicated.

as amino acids, lipids, glucose, and ketone bodies (37). Considering the critical role of starvation in autophagy, we performed comparative analyses of wild-type and *Fam134b*$^{-/-}$ mice (29). Starvation for 48 h resulted in the accumulation of LC3B-I, as well as the autophagy-associated LC3B-II form in the livers of wild-type mice. A similar accumulation was observed in *Fam134b*$^{-/-}$ animals even in the absence of starvation (Supplemental Fig. S1), which implies a possibly disturbed autophagic flux. The stimulated expression of FAM134B-2 in the muscle and heart but not in the pancreas and stomach strongly indicates a possible involvement of this protein in the physiological response against nutrient starvation.

The FAM134B-2 protein, which was weakly positive in the liver of fed animals, was induced strongly by starvation, as reported previously (23). However, besides the verification of the previously reported FAM134B-2 increase at 50 kDa, we surprisingly observed another specific band at 35 kDa, which was also increased upon nutrient starvation, not only in the liver but also in the muscle and heart. Indeed, this shorter isoform could be a post translational modification of FAM134B-2, as well as a protein product of short isoform transcripts.

The starvation-induced FAM134B accumulation in different tissues urged us to carry out a series of analyses to compare wild-type and *Fam134b*$^{-/-}$ mice under fed and starved conditions. *Fam134b*$^{-/-}$ mice under fed conditions did not differ from wild-type animals, with the exception of decreased serum HDL cholesterol levels. Since HDL production and clearance from blood are primarily performed by the liver (39), hepatic FAM134B-2 might be involved in the regulation and/or maturation of HDL particles.

After 36 h of starvation, both wild-type and *Fam134b*$^{-/-}$ mice displayed significant weight loss in total body as well as in liver. Although we found some significant differences in other tissues, the weight loss was less pronounced. There were also

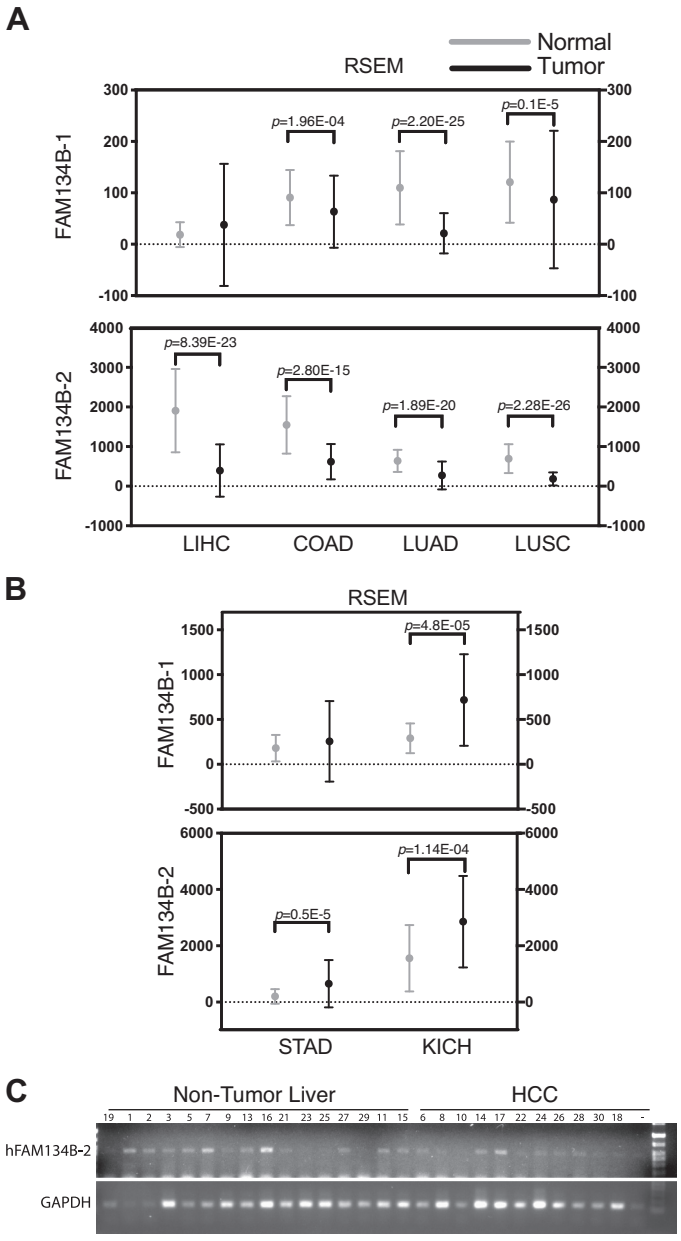

Fig. 11. Significant changes in the expression of FAM134B-1 and FAM134B-2, respectively, in different cancers. *A*: whisker plot of human *FAM134B* isoform levels in hepatocellular carcinoma (LIHC), colon adenocarcinoma (COAD), lung adenocarcinoma (LUAD), and lung squamous carcinoma (LUSC). *B*: whisker plot of human *FAM134B* isoform levels in stomach adenocarcinoma (STAD) and kidney chromophobe cancer (KICH). In *A* and *B*, means ± SD of RNA levels are represented as RNA-Seq by Expectation Maximization (RSEM) values that have been calculated using the data available at the TSVdb database. $P \geq 0.01$ were considered as nonsignificant and not shown on the figure. *C*: confirmation of FAM134B-2 expression in hepatocellular carcinoma (HCC). *Lanes 1–3* represent healthy liver samples; *lanes 5*, *7*, *9*, *13*, *16*, *21*, *23*, *25*, *27*, and *29* are cirrhotic liver, and *lanes 6*, *8*, *10*, *14*, *17*, *22*, *24*, *26*, *28*, and *30* are HCC samples paired with cirrhosis samples in the same order. Total RNA extracted from respective tissues was converted to cDNA and amplified by PCR, using selective primers for FAM134B-1 and FAM134B-2, respectively. GAPDH was used as control.

significant changes in blood parameters, in line with the literature (20, 31, 41).

When we compared starvation responses of wild-type and mutant mice, we identified several important aberrations associated with *Fam134b* deficiency. First, mutant mice were significantly more resistant to body weight loss, as opposed to wild-type mice. Second, mutant mice showed profound aberrations in serum amino acid dynamics. As reported previously, starvation-induced hypoglycemia and a decrease in insulin levels with maintained glucagon levels triggers an autophagic response in the liver, resulting in a surge of amino acids released into the blood at around 24 h of fasting (12). Accordingly, we observed an increase in the serum levels of alanine, asparagine, glycine, lysine, glutamine, serine, tryptophan, and threonine with wild-type mice. In contrast, mutant mice failed to elevate the levels of all these amino acids with only one exception. This observation strongly suggests that in the absence of FAM134B-2, liver tissue cannot undergo sufficient autophagic proteolysis to produce these amino acids. Another interesting observation with *Fam134b*$^{-/-}$ mice was a decrease in the serum levels of methionine, valine, tyrosine, histidine, and proline. Thus it appears that these normal constituents of serum are depleted during starvation, probably because they are converted to glucose. Such a compensation may be necessary when autophagic degradation of proteins is defective.

Glucagon in circulation is one of the key factors for energy mobilization upon nutrient starvation (12). Glucagon was previously shown to downregulate serum calcium levels by altering the gastrointestinal uptake (1). The steady-state calcium levels in mutant mice during starvation strongly suggest a function in calcium homeostasis, likely through intestinal absorption. Finally, *Fam134b*$^{-/-}$, but not wild-type mice, displayed abnormal increases in blood α-amylase levels upon starvation, which indicates pancreatic injury, salivary gland malfunction, or other intraabdominal inflammations (28). As demonstrated in Western blot experiments, FAM134B-2 is predominantly expressed in the pancreas, in which basal autophagy is necessary to maintain α-amylase secreting acinar cells (2). Furthermore, another ER-phagy receptor, CCPG-1, was shown to be critically involved in secretory acinar cells, and its absence results in the accumulation of insoluble α-amylase particles and unfolded protein response (35). Therefore, the α-amylase increase in *Fam134b*$^{-/-}$ could be partially attributed to a defective ER-phagy, which may lead to a discharge or leak of excessive α-amylase into the bloodstream.

Our comprehensive analysis of *FAM134B-1* and *FAM134B-2* expression in the TCGA tumor collection has clearly established that *FAM134B-2* and to a lesser degree *FAM134B-1*, are closely involved in cancer. The loss of *FAM134B-2* expression was observed in HCC, colon, and lung cancers. In contrast, stomach and chromophobe renal cell carcinomas displayed a significant upregulation of the same transcript. *FAM134B-1* levels were generally low in nontumor tissues, but a significant loss was observed in colon and lung cancers, as well as a significant increase in chromophobe renal cell carcinomas. Thus cancers can be grouped into three classes depending on *FAM134B-2* gene expression; those with significant downregulation such as HCC, colon, and lung cancers, those with significant upregulation such as stomach and a subtype of kidney cancers, and those with the *FAM134-2* expression likely not changing significantly in the third group of remaining cancers.

The past few years have been fruitful for the understanding of the molecular roles of *FAM134B,* but without defining its isoforms and their relevance in the whole organism. To our knowledge, this is the first paper to define the differential expression of *FAM134B* isoforms in various tissues under normal and starved conditions, as well as in cancer. These findings greatly help us further understand the functional roles of *FAM134B* isoforms in diseases such as cancer.

ACKNOWLEDGMENTS

We thank the Izmir Biomedicine and Genome Center-Vivarium Rodent Facility and the optical imaging core facility for great support in the experimental procedures. We are also deeply grateful to Deniz Donmez for efforts in improving the manuscript's language. We also thank Christian Hübner for kind donation of *Fam134b*$^{-/-}$ animals.

GRANTS

This study is supported by Dokuz Eylul University, Department of Scientific Research Projects (with the Project code 2014.KB.SAG.047), and Izmir Biomedicine and Genome Center's (IBG) institutional funds. The Genotype-Tissue Expression (GTEx) Project was supported by the Common Fund of the Office of the Director of the National Institutes of Health and by the National Cancer Institute, National Human Genome Research Institute, National Heart, Lung, and Blood Institute, National Institute on Drug Abuse, National Institute of Mental Health, and National Institute of Neurological Disorders and Stroke. The data used for the analyses described in this article were obtained from the GTEx Portal on 11/14/2018 and/or dbGaP Accession No. phs000424.v3.p1.

DISCLOSURES

No conflicts of interest, financial or otherwise, are declared by the authors.

AUTHOR CONTRIBUTIONS

U.K., M.O., E.I. conceived and designed research; U.K., Z.M., S.K.,M.A.S., N.A., M.O., E.I., H.E.Y., G.K., E.B., N.T., A.C. and U.E. performed experiments; U.K., G.K.,A.S. and E.B. analyzed data; U.K., M.A.S., M.O., E.I., H.E.Y., G.K., A.S. and E.B. interpreted results of experiments; U.K. and E.I. prepared figures; U.K., M.O., E.I. drafted manuscript; U.K., Z.M., S.K., M.A.S., N.A., M.O., E.I., H.E.Y., G.K., A.S., E.B., N.T., A.C. and U.E. edited and revised manuscript; U.K., Z.M., S.K., N.A., M.O., E.I., H.E.Y., G.K., A.S., E.B., N.T., A.C. and U.E. approved final version of manuscript.

REFERENCES

1. **Aliapoulios MA**, **Morain WD**, **Kacoyanis GP.** Glucagon as a hypocalcemic and hypophosphatemic agent in the rat. *Gastroenterology* 65: 912–918, 1973. doi:10.1016/S0016-5085(19)32984-1.
2. **Antonucci L**, **Fagman JB**, **Kim JY**, **Todoric J**, **Gukovsky I**, **Mackey M**, **Ellisman MH**, **Karin M.** Basal autophagy maintains pancreatic acinar cell homeostasis and protein synthesis and prevents ER stress. *Proc Natl Acad Sci USA* 112: E6166–E6174, 2015. doi:10.1073/pnas.1519384112.
3. **Ardlie KG**, **DeLuca DS**, **Segrè AV**, **Sullivan TJ**, **Young TR**, **Gelfand ET**, et al; **GTEx Consortium.** Human genomics. The Genotype-Tissue Expression (GTEx) pilot analysis: multitissue gene regulation in humans. *Science* 348: 648–660, 2015. doi:10.1126/science.1262110.
4. **Bashour AM**, **Bloom GS.** 58K, a microtubule-binding Golgi protein, is a formiminotransferase cyclodeaminase. *J Biol Chem* 273: 19612–19617, 1998. doi:10.1074/jbc.273.31.19612.
5. **Bateman A**; **UniProt Consortium.** UniProt: a worldwide hub of protein knowledge. *Nucleic Acids Res* 47, D1: D506–D515, 2019. doi:10.1093/nar/gky1049.
6. **Bhaskara RM**, **Grumati P**, **Garcia-Pardo J**, **Kalayil S**, **Covarrubias-Pinto A**, **Chen W**, **Kudryashev M**, **Dikic I**, **Hummer G.** Curvature induction and membrane remodeling by FAM134B reticulon homology domain assist selective ER-phagy. *Nat Commun* 10: 2370, 2019. doi:10.1038/s41467-019-10345-3.
7. **Buchan DW**, **Jones DT.** The PSIPRED Protein Analysis Workbench: 20 years on. *Nucleic Acids Res* 47, W1: W402–W407, 2019. doi:10.1093/nar/gkz297.

8. **Cai M**, **Zhao J**, **Liu Q**, **Wang X**, **Wang Y.** FAM134B improves preadipocytes differentiation by enhancing mitophagy. *Biochim Biophys Acta Mol Cell Biol Lipids* 1864: 158508, 2019. doi:10.1016/j.bbalip.2019.08.004.
9. **Charest A**, **Lane K**, **McMahon K**, **Housman DE.** Association of a novel PDZ domain-containing peripheral Golgi protein with the Q-SNARE (Q-soluble *N*-ethylmaleimide-sensitive fusion protein (NSF) attachment protein receptor) protein syntaxin 6. *J Biol Chem* 276: 29456–29465, 2001. doi:10.1074/jbc.M104137200.
10. **Chiurchiù V**, **Maccarrone M**, **Orlacchio A.** The role of reticulons in neurodegenerative diseases. *Neuromolecular Med* 16: 3–15, 2014. doi:10.1007/s12017-013-8271-9.
11. **Dai X**, **Hua T**, **Hong T.** Integrated diagnostic network construction reveals a 4-gene panel and 5 cancer hallmarks driving breast cancer heterogeneity. *Sci Rep* 7: 6827, 2017. doi:10.1038/s41598-017-07189-6.
12. **Ezaki J**, **Matsumoto N**, **Takeda-Ezaki M**, **Komatsu M**, **Takahashi K**, **Hiraoka Y**, **Taka H**, **Fujimura T**, **Takehana K**, **Yoshida M**, **Iwata J**, **Tanida I**, **Furuya N**, **Zheng DM**, **Tada N**, **Tanaka K**, **Kominami E**, **Ueno T.** Liver autophagy contributes to the maintenance of blood glucose and amino acid levels. *Autophagy* 7: 727–736, 2011. doi:10.4161/auto.7.7.15371.
13. **Forrester A**, **De Leonibus C**, **Grumati P**, **Fasana E**, **Piemontese M**, **Staiano L**, **Fregno I**, **Raimondi A**, **Marazza A**, **Bruno G**, **Iavazzo M**, **Intartaglia D**, **Seczynska M**, **van Anken E**, **Conte I**, **De Matteis MA**, **Dikic I**, **Molinari M**, **Settembre C.** A selective ER-phagy exerts procollagen quality control via a Calnexin-FAM134B complex. *EMBO J* 38: 1–16, 2019. doi:10.15252/embj.201899847.
14. **Fregno I**, **Molinari M.** Endoplasmic reticulum turnover: ER-phagy and other flavors in selective and non-selective ER clearance. *F1000 Res* 7: 454, 2018. doi:10.12688/f1000research.13968.1.
15. **Friedewald WT**, **Levy RI**, **Fredrickson DS.** Estimation of the concentration of low-density lipoprotein cholesterol in plasma, without use of the preparative ultracentrifuge. *Clin Chem* 18: 499–502, 1972. doi:10.1093/clinchem/18.6.499.
16. **Fuchs BC**, **Fujii T**, **Dorfman JD**, **Goodwin JM**, **Zhu AX**, **Lanuti M**, **Tanabe KK.** Epithelial-to-mesenchymal transition and integrin-linked kinase mediate sensitivity to epidermal growth factor receptor inhibition in human hepatoma cells. *Cancer Res* 68: 2391–2399, 2008. doi:10.1158/0008-5472.CAN-07-2460.
17. **Gangalum RK**, **Horwitz J**, **Kohan SA**, **Bhat SP.** αA-crystallin and αB-crystallin reside in separate subcellular compartments in the developing ocular lens. *J Biol Chem* 287: 42407–42416, 2012. doi:10.1074/jbc.M112.414854.
19. **Islam F**, **Gopalan V**, **Law S**, **Tang JC**, **Lam AK.** FAM134B promotes esophageal squamous cell carcinoma in vitro and its correlations with clinicopathologic features. *Hum Pathol* 87: 1–10, 2019. doi:10.1016/j.humpath.2018.11.033.
20. **Jensen TL**, **Kiersgaard MK**, **Sørensen DB**, **Mikkelsen LF.** Fasting of mice: a review. *Lab Anim* 47: 225–240, 2013. doi:10.1177/0023677213501659.
21. **Kasem K**, **Gopalan V**, **Salajegheh A**, **Lu CT**, **Smith RA**, **Lam AKY.** The roles of JK-1 (FAM134B) expressions in colorectal cancer. *Exp Cell Res* 326: 166–173, 2014. doi:10.1016/j.yexcr.2014.06.013.
22. **Khaminets A**, **Heinrich T**, **Mari M**, **Grumati P**, **Huebner AK**, **Akutsu M**, **Liebmann L**, **Stolz A**, **Nietzsche S**, **Koch N**, **Mauthe M**, **Katona I**, **Qualmann B**, **Weis J**, **Reggiori F**, **Kurth I**, **Hübner CA**, **Dikic I.** Regulation of endoplasmic reticulum turnover by selective autophagy. *Nature* 522: 354–358, 2015. doi:10.1038/nature14498.
23. **Kohno S**, **Shiozaki Y**, **Keenan AL**, **Miyazaki-Anzai S**, **Miyazaki M.** An N-terminal-truncated isoform of FAM134B (FAM134B-2) regulates starvation-induced hepatic selective ER-phagy. *Life Sci Alliance* 2: 1–13, 2019. doi:10.26508/lsa.201900340.
24. **Korolenko TA**, **Johnston TP**, **Tuzikov FV**, **Tuzikova NA**, **Pupyshev AB**, **Spiridonov VK**, **Goncharova NV**, **Maiborodin IV**, **Zhukova NA.** Early-stage atherosclerosis in poloxamer 407-induced hyperlipidemic mice: pathological features and changes in the lipid composition of serum lipoprotein fractions and subfractions. *Lipids Health Dis* 15: 16, 2016. doi:10.1186/s12944-016-0186-7.
25. **Kurth I**, **Pamminger T**, **Hennings JC**, **Soehendra D**, **Huebner AK**, **Rotthier A**, **Baets J**, **Senderek J**, **Topaloglu H**, **Farrell SA**, **Nürnberg G**, **Nürnberg P**, **De Jonghe P**, **Gal A**, **Kaether C**, **Timmerman V**, **Hübner CA.** Mutations in FAM134B, encoding a newly identified Golgi protein, cause severe sensory and autonomic neuropathy. *Nat Genet* 41: 1179–1181, 2009. doi:10.1038/ng.464.
26. **Lennemann NJ**, **Coyne CB.** Dengue and Zika viruses subvert reticulophagy by NS2B3-mediated cleavage of FAM134B. *Autophagy* 13: 322–332, 2017. doi:10.1080/15548627.2016.1265192.
27. **Liao Y**, **Duan B**, **Zhang Y**, **Zhang X**, **Xia B.** Excessive ER-phagy mediated by the autophagy receptor FAM134B results in ER stress, the unfolded protein response, and cell death in HeLa cells. *J Biol Chem* 294: 20009–20023, 2019. doi:10.1074/jbc.RA119.008709.
28. **Matull WR**, **Pereira SP**, **O'Donohue JW.** Biochemical markers of acute pancreatitis. *J Clin Pathol* 59: 340–344, 2006. doi:10.1136/jcp.2002.002923.
29. **Mizushima N**, **Yamamoto A**, **Matsui M**, **Yoshimori T**, **Ohsumi Y.** In vivo analysis of autophagy in response to nutrient starvation using transgenic mice expressing a fluorescent autophagosome marker. *Mol Biol Cell* 15: 1101–1111, 2004. doi:10.1091/mbc.e03-09-0704.
30. **Nakamura N**, **Rabouille C**, **Watson R**, **Nilsson T**, **Hui N**, **Slusarewicz P**, **Kreis TE**, **Warren G.** Characterization of a cis-Golgi matrix protein, GM130. *J Cell Biol* 131: 1715–1726, 1995. doi:10.1083/jcb.131.6.1715.
31. **Namazi F**, **Omidi A**, **Abbasi S**, **Afsar M**, **Honarmand M**, **Nazifi S.** Starvation and refeeding in rats: Effect on some parameters of energy metabolism and electrolytes and changes of hepatic tissue. *Pesqui Vet Bras* 36, Suppl 1: 101–105, 2016. doi:10.1590/S0100-736X2016001300015.
32. **Nugent T**, **Jones DT.** Transmembrane protein topology prediction using support vector machines. *BMC Bioinformatics* 10: 159, 2009. doi:10.1186/1471-2105-10-159.
33. **Okazaki Y**, **Ohno H**, **Takase K**, **Ochiai T**, **Saito T.** Cell surface expression of calnexin, a molecular chaperone in the endoplasmic reticulum. *J Biol Chem* 275: 35751–35758, 2000. doi:10.1074/jbc.M007476200.
34. **Reverter M**, **Rentero C**, **Garcia-Melero A**, **Hoque M**, **Vilà de Muga S**, **Álvarez-Guaita A**, **Conway JRW**, **Wood P**, **Cairns R**, **Lykopoulou L**, **Grinberg D**, **Vilageliu L**, **Bosch M**, **Heeren J**, **Blasi J**, **Timpson P**, **Pol A**, **Tebar F**, **Murray RZ**, **Grewal T**, **Enrich C.** Cholesterol regulates Syntaxin 6 trafficking at trans-Golgi network endosomal boundaries. *Cell Reports* 7: 883–897, 2014. doi:10.1016/j.celrep.2014.03.043.
35. **Smith MD**, **Harley ME**, **Kemp AJ**, **Wills J**, **Lee M**, **Arends M**, **von Kriegsheim A**, **Behrends C**, **Wilkinson S.** CCPG1 Is a Non-canonical Autophagy Cargo Receptor Essential for ER-Phagy and Pancreatic ER Proteostasis. *Dev Cell* 44: 217–232.e11, 2018. doi:10.1016/j.devcel.2017.11.024.
36. **Sun W**, **Duan T**, **Ye P**, **Chen K**, **Zhang G**, **Lai M**, **Zhang H.** TSVdb: a web-tool for TCGA splicing variants analysis. *BMC Genomics* 19: 405, 2018. doi:10.1186/s12864-018-4775-x.
37. **Takagi A**, **Kume S**, **Kondo M**, **Nakazawa J**, **Chin-Kanasaki M**, **Araki H**, **Araki S**, **Koya D**, **Haneda M**, **Chano T**, **Matsusaka T**, **Nagao K**, **Adachi Y**, **Chan L**, **Maegawa H**, **Uzu T.** Mammalian autophagy is essential for hepatic and renal ketogenesis during starvation. *Sci Rep* 6: 18944, 2016. doi:10.1038/srep18944.
38. **Tang WK**, **Chui CH**, **Fatima S**, **Kok SH**, **Pak KC**, **Ou TM**, **Hui KS**, **Wong MM**, **Wong J**, **Law S**, **Tsao SW**, **Lam KY**, **Beh PS**, **Srivastava G**, **Chan AS**, **Ho KP**, **Tang JC.** Oncogenic properties of a novel gene JK-1 located in chromosome 5p and its overexpression in human esophageal squamous cell carcinoma. *Int J Mol Med* 19: 915–923, 2007. doi:10.3892/ijmm.19.6.915.

38a. **Thibert V**, **Netter C**, **Hautem J**, **Saintier A**, **Thioulouse E**, **Couderc R**, **Moussa F.** Direct quantification of amino acids in plasma by liquid chromatography-tandem mass spectrometry for clinical research. *ThermoScientific Tech Note 65382*. https://assets.thermofisher.com/TFS-Assets/CMD/Technical-Notes/tn-65382-lc-ms-amino-acids-plasma-tn65382-en.pdf.

39. **Trieb M**, **Horvath A**, **Birner-Gruenberger R**, **Spindelboeck W**, **Stadlbauer V**, **Taschler U**, **Curcic S**, **Stauber RE**, **Holzer M**, **Pasterk L**, **Heinemann A**, **Marsche G.** Liver disease alters high-density lipoprotein composition, metabolism and function. *Biochim Biophys Acta* 1861: 630–638, 2016. doi:10.1016/j.bbalip.2016.04.013.
40. **Wang L**, **Wang Y**, **Liang Y**, **Li J**, **Liu Y**, **Zhang J**, **Zhang A**, **Fu J**, **Jiang G.** PFOS induced lipid metabolism disturbances in BALB/c mice through inhibition of low density lipoproteins excretion. *Sci Rep* 4: 4582, 2014. doi:10.1038/srep04582.
41. **Yamamoto J**, **Kamata S**, **Miura A**, **Nagata T**, **Kainuma R**, **Ishii I.** Differential adaptive responses to 1- or 2-day fasting in various mouse tissues revealed by quantitative PCR analysis. *FEBS Open Bio* 5: 357–368, 2015. doi:10.1016/j.fob.2015.04.012.
42. **Yildiz G**, **Arslan-Ergul A**, **Bagislar S**, **Konu O**, **Yuzugullu H**, **Gursoy-Yuzugullu O**, **Ozturk N**, **Ozen C**, **Ozdag H**, **Erdal E**, **Karademir S**, **Sagol O**, **Mizrak D**, **Bozkaya H**, **Ilk HG**, **Ilk O**, **Bilen B**, **Cetin-Atalay R**, **Akar N**, **Ozturk M.** Genome-wide transcriptional reorganization associated with senescence-to-immortality switch during human hepatocellular carcinogenesis. *PLoS One* 8: e64016, 2013. doi:10.1371/journal.pone.0064016.

43. **Yuan Z**, **Song D**, **Wang Y.** The novel gene pFAM134B positively regulates fat deposition in the subcutaneous fat of Sus scrofa. *Biochem Biophys Res Commun* 454: 554–559, 2014. doi:10.1016/j.bbrc.2014.10.117.
44. **Yuzugullu H**, **Benhaj K**, **Ozturk N**, **Senturk S**, **Celik E**, **Toylu A**, **Tasdemir N**, **Yilmaz M**, **Erdal E**, **Akcali KC**, **Atabey N**, **Ozturk M.** Canonical Wnt signaling is antagonized by noncanonical Wnt5a in hepatocellular carcinoma cells. *Mol Cancer* 8: 90, 2009. doi:10.1186/1476-4598-8-90.
45. **Zhang ZQ**, **Chen J**, **Huang WQ**, **Ning D**, **Liu QM**, **Wang C**, **Zhang L**, **Ren L**, **Chu L**, **Liang HF**, **Fan HN**, **Zhang BX**, **Chen XP.** FAM134B induces tumorigenesis and epithelial-to-mesenchymal transition via Akt signaling in hepatocellular carcinoma. *Mol Oncol* 13: 792–810, 2019. doi:10.1002/1878-0261.12429.
46. **Zhou X**, **He Y**, **Huang X**, **Guo Y**, **Li D**, **Hu J.** Reciprocal regulation between lunapark and atlastin facilitates ER three-way junction formation. *Protein Cell* 10: 510–525, 2019. doi:10.1007/s13238-018-0595-7.